

# Analysis of perturbative effects of a momentum flux probe in a plasma plume

Séverin ASTRUC\*<sup>†</sup> and Paul-Quentin ELIAS\*

\* DPHY, ONERA

Université Paris-Saclay, F-91123 Palaiseau, France

[severin.astruc@onera.fr](mailto:severin.astruc@onera.fr) – [paul-quentin.elias@onera.fr](mailto:paul-quentin.elias@onera.fr)

<sup>†</sup> Corresponding Author

## Abstract

One way to measure the thrust of an electric thruster is to use a probe measuring the momentum flux in the plasma plume. One can ask how the probe alters the plasma properties and if the momentum flux measurement remains accurate. In this study, we address this issue by considering a cold gas source. Experimental momentum flux measurements are compared to a Direct Simulation Monte-Carlo of the experiment. We show that the momentum flux measurements depend on the nature of the interaction between the particles and the probe surface. Additionally, the design of the housing protecting the sensor can increase particles' backflow and alter the measure. Therefore, to have an accurate momentum flux measurement, the sensing part of the sensor needs to be exposed to the plume without a casing nearby.

## 1. Introduction

The use of electric thrusters on satellite platforms is increasing. Electric thrusters are more efficient than conventional thrusters owing to their larger specific impulse, but this technology is characterized by a low thrust-to-weight ratio and vacuum use only. The thrust is one of their most important performance parameters; measuring it during ground testing can be challenging. One of the most used ways is the thrust balance [2]. In this configuration, the thruster is mounted on a pendulum inside a vacuum chamber. The thruster is mounted on the free end of the pendulum arm; the other end is fixed to the vacuum tank. When the thruster is powered on, the thrust force deflects the pendulum. After calibration, a measure of the pendulum displacement yields the thrust. Unfortunately, some test conditions or thruster configurations prevent the use of such balances. Another way to measure the thrust is to measure the momentum flux in the plasma plume with a probe. This probe is constituted of a target, which intercepts the plasma [1], disposed at the end of an arm. The other end of the arm is also fixed to the vacuum tank. Like a pendulum, the target measures the thrust by its deflection.

The thrust measured by these probes is in good agreement with balance measurements [3] in the case of thrust larger than 100mN, with only 6% difference between both measurements. It can reach 1.8% for Zhang et al [4] in a 15mN thrust. West et al [5] developed a high-sensitivity target on the low thrust spectrum to measure a force as low as 15 $\mu$ N. The sensitivity of these pendulums depends on the length of a pendulum arm and the large size of the target. The size of the vacuum tank can constrain both of these dimensions. To avoid this issue, more compact thrust probes exist for low thrust. First, it is possible to reduce the size of the target arm system. Trottenberg et al [6] designed a compact target (diameter of 1.5cm) with an arm of 10.5 cm. A galvanometer transduces the target displacement to a voltage. A calibration of the target yields the thrust. Nevertheless, the size of the probe remains comparable to the thruster. Chakraborty et al [7] used a target with hinges instead of the arm. A force sensor measures the target (45x45mm<sup>2</sup>) displacement in this configuration. Finally, Seo et al designed a target with the sensing instrument directly on the target [8]. A strain gauge measures the target deformation thanks to a piezoresistive sensing method. This probe is more compact than the previous one but, for the moment, it cannot operate in a plasma plume because of the non-protected electrodes.

All of these compact probes need a sensor shielded from the plasma. In the case of Chakraborty, this shielding is achieved by intercepting the entire plasma plume with the target. Unfortunately, the sensor position and size depend on the plasma plume geometry and thruster characteristics. On the contrary, Trottenberg protects its probe with a housing to measure the momentum flux at any given point of the plasma plume. However, introducing such a complex probe design in the thruster plume perturbs the plasma. One can ask how the probe alters the plasma properties and if the momentum flux measurement remains accurate.

To address these issues, we have proposed to use a highly sensitive miniature MEMS sensor to measure the momentum flux in a plasma thruster plume [9], [10]. To demonstrate the use of such a probe to measure the thrust of a plasma thruster, several issues need to be addressed. First, is the probe sensitive enough to achieve an accurate measurement? Second, what is the effect of sensor casing on the measurements? Third, to what extent do the perturbations induced by the probe modify the momentum flux measurement? In this study, we address the first two questions by considering a simplified case where plasma perturbations are absent. For this purpose, we first measure the momentum flux of a cold gas source in a vacuum chamber. The highly sensitive probe measures the radial pressure profile in the cold gas jet. This probe comprises a custom-built MEMS accelerometer mounted on a metal housing [10]. Experimental data are then compared to a simulation of the experiment performed with a Direct Simulation Monte-Carlo code. We show that the momentum flux measurements depend on the nature of the interaction between the particles and the probe surface. This interaction can be diffusive or specular, depending on the material. Additionally, the design of the housing protecting the sensor can increase particles' backflow and alter the measure. Therefore, to have an accurate momentum flux measurement, the sensing part of the sensor needs to be exposed to the plume without a casing nearby. Work on the design of the case is necessary. These first results in a neutral environment are essential to understand the probe behavior in a plasma plume. In addition, other effects, such as a plasma sheath and an electrostatic pressure, will appear and need to be assessed.

## 2. Models and methods

We have developed a custom-built probe to understand the force probe's behavior in a plasma jet. It is composed of an accelerometer encapsulated in a shielded box. This accelerometer is made from a 500 $\mu\text{m}$  thick monocrystalline quartz wafer. As shown in Figure 1, it is composed of a proof mass linked to the sensor frame by two hinges and a vibrating beam. These three links are 30 $\mu\text{m}$  thick. The beam is located on one side of the wafer, while the hinges are on the other. When an acceleration or a force is applied to the proof mass, it rotates around the hinges and transmits a force on the beam, as explained in Figure 2. This force changes the vibrating frequency of the beam. This drift in frequency is directly linked to the force applied to the proof mass [11]. The sensor is connected to six pins, which are welded to a PCB card. This card holds the proximity electronics necessary to the sensor operation. A venting hole behind the proof mass limits the pressure build-up from plasma particles. A metal coating on the PCB face and the proof mass keeps the sensor at the same potential as the probe assembly. This avoids an electrostatic charge build-up and the creation of a spurious electrostatic force. The PCB and the sensor are mounted inside a shielded box, as shown in Figure 3.

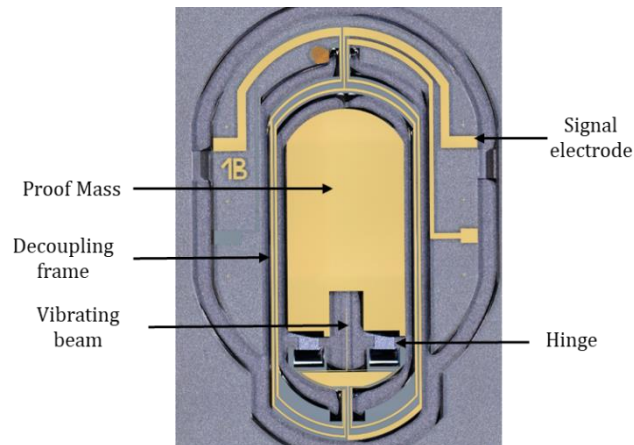


Figure 1: Front side microscope photograph of the quartz accelerometer. It is composed of a proof mass linked to a decoupling frame by two hinges and one vibrating beam. The quartz is transparent but appears in grey here; gold electrodes are deposited on the quartz and appear in yellow. The sensor is 20mm high for 0.5mm in thickness

The probe is mounted on a translation stage and can be centred in front of the source in this configuration. The translation stage enables positioning the probe at any point in front of the plasma source along a displacement line, see Figure 4. If we assume an axial symmetry of the plume pressure, then the pressure along this line can represent the pressure at any given point. The whole setup is placed inside the ONERA B09 vacuum tank. This vacuum tank is a stainless steel cylinder with a radius of 80cm and 2m in length. Fitted with a primary pump, three turbomolecular

pumps, and a cryogenic pump, the facility ultimate pressure is as low as  $10^{-7}$  mbar with a pump velocity of 12 000  $\text{L}\cdot\text{s}^{-1}$ .

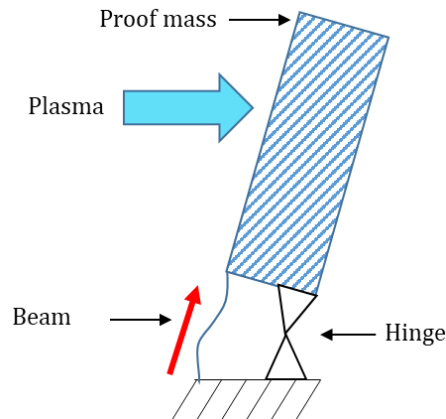


Figure 2: Schematic side view of the sensor. When the plasma impinges the proof mass, it rotates around the hinge and creates a force on the beam proportional to the plasma force

This probe was exposed in front of an electron-cyclotron resonance thruster, and the results were presented in a previous paper [10]. We showed that the sensor measured a plasma pressure higher than expected. One of the hypotheses was that there was a non-negligible effect of the shielding. Particles from the plasma accumulate inside the probe casing, and apply a local pressure on one side of the proof mass. Thus, force measured during the experiment came from the direct plasma pressure of the thruster but also the local pressure inside the casing. Here we change the plasma thruster with a neutral gas source to remove the plasma's harsh conditions (thermal flux, electrostatic charges). This source comprises an argon tank at 150 bar, and a two-stage regulator to get a  $\sim 1$  bar pressure inside a feeding pipe. The gas is then directed to a mass flow rate controller letting around  $\dot{m} \approx 0.2$  mg/s of argon through a  $\Phi_0 = 8$  mm diameter thin aperture. This flow is chosen to create a plume of neutral gas in a free molecular flow (Knudsen number  $\text{Kn} > 1$ ). The probe is located 130 mm downstream of the aperture in a cylindrical section with a radius of 75 mm. It can be displaced along a line crossing the centre axis of the source.



Figure 3: Two sensors mounted on the PCB card. This card is golded to be conductor. The PCB is placed inside the shielded boxes. The whole setup is hold by a translation stage behind (blurred here)

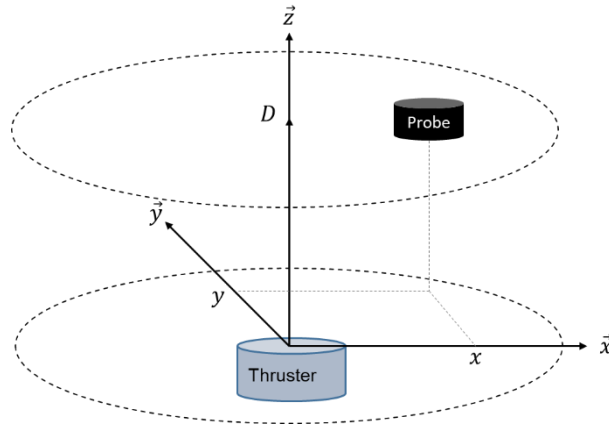


Figure 4: Schematic view of the principle of a scan of the plasma pressure

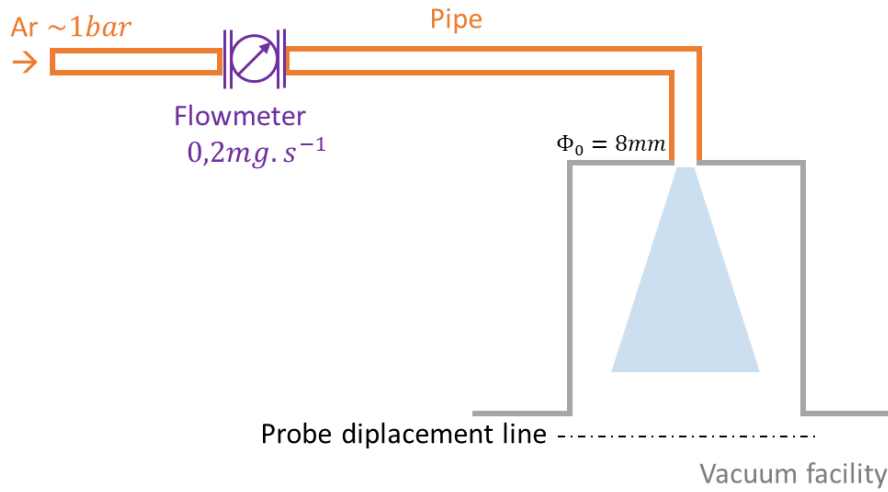


Figure 5: Schematic diagram of the experiment

Here, we have an upstream gas in a continuous regime flowing through an aperture in a near vacuum. This configuration is similar to a choked flow through an aperture because the downstream pressure  $P_1$  is lower than the critical pressure  $P^*$ .  $P^*$  can be written depending of only the upstream pressure  $P_0$ .

$$\frac{P^*}{P_0} = \left( \frac{2}{\gamma + 1} \right)^{\frac{\gamma}{\gamma - 1}} = 0.49 \quad (1)$$

With the heat capacity ratio of the Argon  $\gamma = 1.66$  assuming a perfect gas [12].

At room temperature ( $T_0 = 293 \text{ K}$ ), because the flow is choked, the downstream velocity of argon particles is limited to

$$c_d = \left( \frac{\gamma R}{M_{Ar}} T_0 \right)^{1/2} = 317 \text{ m.s}^{-1} \quad (2)$$

With the molar mass of argon particle  $M_{Ar} = 39.95 \text{ g.mol}^{-1}$ , and the gas constant  $R = 8,314 \text{ J.K}^{-1}.\text{mol}^{-1}$ . Given the mass flow rate  $\dot{m}$ :

$$\dot{m} = \frac{\psi^* A^* P_0}{c_d} \quad (3)$$

With

$$\psi^* = \gamma \left( \frac{2}{\gamma + 1} \right)^{\frac{\gamma+1}{2(\gamma-1)}} = 0.93 \quad (4)$$

And the aperture section

$$A^* = \pi \times \left( \frac{\Phi_0}{2} \right)^2 \quad (5)$$

And because the mass flow  $\dot{m}$  is controlled, the downstream pressure is lower than the critical pressure

$$P_1 < P^* = 0,49 \frac{\dot{m} c_i}{\psi^* A^*} = 66 \mu N \cdot cm^{-2} \quad (6)$$

To determine the rarefaction of the flow, we can use the Knudsen number  $K_n$ , [13]:

$$K_n = \frac{\eta}{P^* \Phi_0} \left( \frac{\pi R_0 T}{2 m_{Ar}} \right)^{1/2} = \frac{1}{P d} \times 6,9 \times 10^{-3} \quad (7)$$

With the argon viscosity  $\eta = 2.23 \times 10^{-5} Pa \cdot s$  at room temperature and an argon particle mass  $m_{Ar} = 6.6 \times 10^{-26} kg$ , the Knudsen number at a position just after the aperture is higher than 1.3. According to Lafferty [13], a Knudsen number higher than 0.5 give a flow in the free molecular flow regime. With this kind of flow, it is possible to use a statistical numeric method to simulate the experiment. We use a Direct Simulation Monte Carlo (DSMC) method. In this numeric method, particles trajectory are computed by solving the Boltzmann equation with probabilistic methods. At each time step, a new position of the particles is computed, then probabilistic models simulate the collision. Here we use the code DS2V, [14].

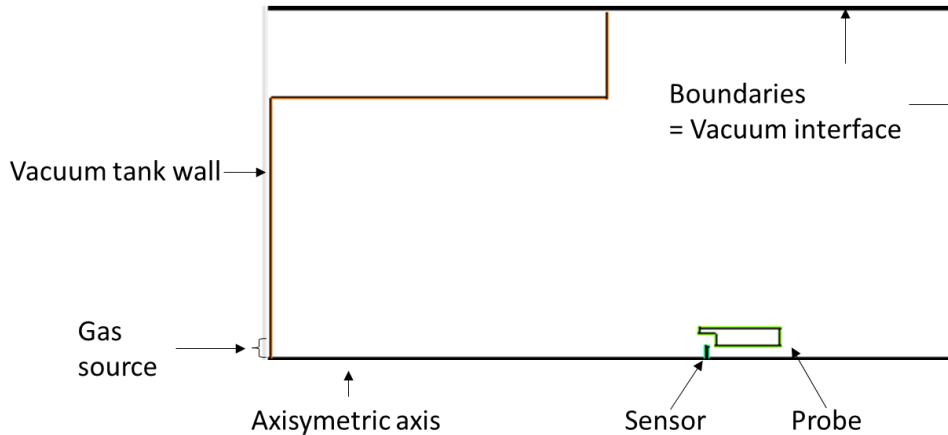


Figure 6: Geometric view of the simulation of the probe, the sensor and the model boundaries.

The previous experiment is modeled in a 2D axisymmetric simulation. As shown in Figure 6, it comprises the gas source and the vacuum tank (radius of 75mm) on the left boundary. A cylinder of 75mm of radius represents the rest of the vacuum tank. On the upper and right side of the simulation, the boundaries remain open to simulate the vacuum tank at a great distance from the gas source. Then, three different cases were simulated. In the first case, only the vacuum tank and the source exist. This case is a reference to understand the change when introducing the probe. It is named “without sensor”. The second case has a sensor of 0.5mm of thickness and 3.5mm of radius at 13cm from the source. This case is named “with sensor”. The last one, a 20 mm thick ring, is added behind the sensor to represent the shield provided by the case. This ring has an inner radius of 3mm and an outer radius of 6.5mm. This one is named “with probe”. The tank, probe, and sensor have diffusive boundary conditions.

In the experiment, the particle mass flow  $\dot{m}$  is the only control parameter of the source. This term is linked to the particle flux  $\Phi$  by the knowledge of the aperture surface and the argon particle mass  $\dot{m}_{Ar}$ .

$$\Phi = \frac{\dot{m}}{A \cdot m_{Ar}} \text{ [particles/m}^2\text{/s]} \quad (8)$$

However, in the DS2V source, particles come from a virtual reservoir and exhaust outside the source boundary. The gas temperature and the gas density characterize the source. The temperature is simply defined as the temperature of the room,  $T_0 = 293K$ . To select the proper gas density, we can use the particle flux  $\Phi$  in free molecular regime [15] :

$$\Phi = \frac{1}{4} n \bar{v} \text{ [particles/m}^2\text{/s]} \quad (9)$$

With  $\bar{v}$  the particle average velocity

$$\bar{v} = \left( \frac{8kT_0}{\pi m_{Ar}} \right)^{1/2} = 394 \text{ m/s} \quad (10)$$

Therefore, the density at the source is

$$n = \frac{4}{\bar{v}} \frac{\dot{m}}{A \cdot m_{Ar}} = 8.52 \times 10^{20} \text{ m}^{-3} \quad (11)$$

The particles flow downstream to the source. At a given position  $\vec{r}$ , the pressure exerted by the particles depends on the temperature  $T(\vec{r})$ , and the number density of the gas  $n(\vec{r})$ . As the fluid has a mean velocity  $u$ , a dynamic term appears in the pressure.

$$P(\vec{r}) = n(\vec{r})kT(\vec{r}) + \rho(\vec{r})u^2 \quad (12)$$

Now consider a thin plate at rest immersed in the fluid. Its two faces normal vectors are parallel to direction of the fluid, as shown in Figure 7. The surface oriented in the direction of the moving fluid is named Surface 1, and the other is named Surface 2. There are two different interactions possible when a particle impinges the surface 1. The particle comes with an incidence angle from the surface's normal direction. In the first case, the particle is reflected at the same angle. It is a specular reflection. In this case, the particle momentum in the normal direction is inverted. By conservation of the momentum, the surface gets two times the projection along  $n$  of particle momentum. In the second case, the particles are reflected at random angles in a diffusive reflection. In such reflection, the reflected particle momentum in the normal direction is not the same amplitude as the incident one. Surface 1 gets less than two times the incident particle momentum in the normal axis. For a uniform particle flux in the vacuum, no particle hits the surface 2. However, if a surface is behind the plate, the flux hitting surface 2 exists and follows the same law as surface 1.

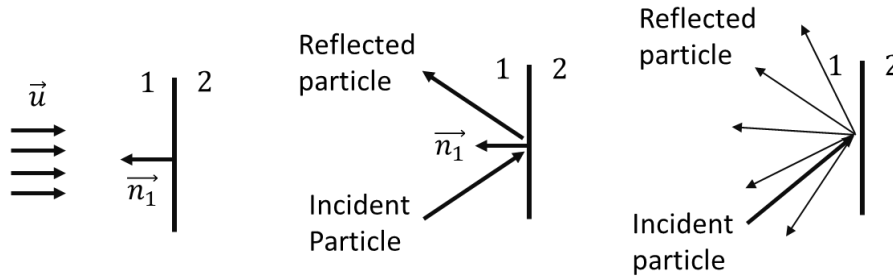


Figure 7: Sketch of the specular and the diffusive model of the interaction between an interface and a particle.

### 3. Results

#### 3.1 Results from experiment

The first measure consists of a plume pressure measurement. The probe translates from 5 cm to the right of the source to 5 cm to the left. The probe stops each half a centimetre to measure the pressure of the plume. This measurement is repeatable and made four times to improve accuracy. Figure 8 shows the pressure measured by the sensor and measurement uncertainty at the different positions. This uncertainty is computed from the standard deviation of the four measurements. It could be improved by increasing the number of measures. A zero pressure means that no particles hit the sensor. This result is shaped as a bell centred in the axis position with a maximum of  $0.328 \pm 0.002 \mu N \cdot cm^{-2}$ . The bell is nearly symmetric around the centre axis. The pressure drops to  $0.253 \pm 0.001 \mu N \cdot cm^{-2}$  on the left side and  $0.237 \pm 0.001 \mu N \cdot cm^{-2}$  on the right side.

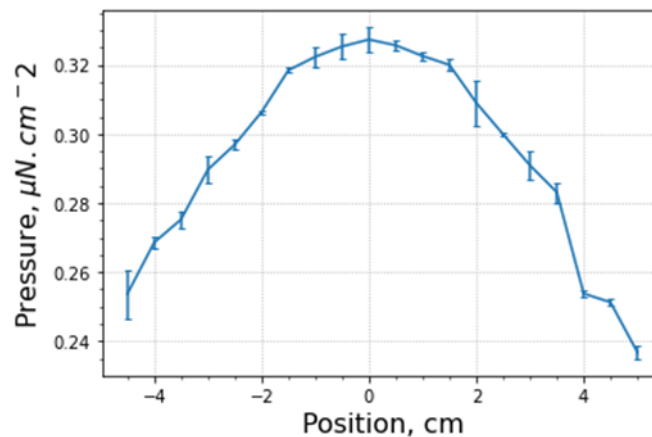


Figure 8: Sensor frequency change when translating from -5cm to +5cm from the source axis

#### 3.2 Results from DS2V simulation

Here, the experiment is simulated with the DS2V code. We can see in Figure 9 the pressure map for three different cases. The first one is only composed of the source, and we can see three different pressure regions. The source acts as a point source, and the pressure decrease in the radial and axial direction to reach half its highest value. Therefore, the pressure decreases from  $13 \times 10^{-3} N \cdot m^{-2}$  to  $7 \times 10^{-3} N \cdot m^{-2}$ . After this region, the pressure is constant along the radial direction. There is a pressure drop at the exit of the cylindrical section, and the pressure becomes almost zero only a few centimeters downstream of the cylinder exit section. In the middle figure, a sensor is added. This sensor changes the local gas behavior. There is an increase in the pressure in front of the sensor. Behind it, there are no particles. In the last simulation, a case is added around the sensor. This case has a complex geometry. In fact, it increases sharply the pressure around and behind the sensor.

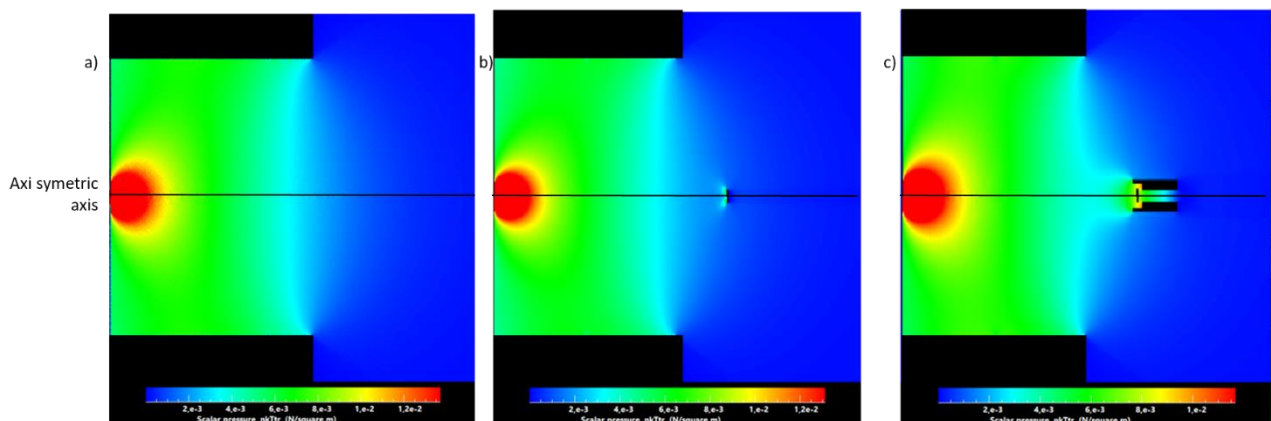


Figure 9: Pressure in front of the gas source simulated with the 2D axisymmetric DS2V code. There is three case. Left: without sensor. Center: with the sensor. Right: with the probe

To understand the pressure measured by the sensor, Figure 10 shows the pressure applied by the gas on the front face of the sensor and the back face of the sensor. The first case, on the left, shows the pressure when no case exists around the sensor. The pressure applied on the front face is nearly constant at  $1.00 \mu N \cdot cm^{-2}$  in average. No particles are hitting the sensor's back face, so there is no pressure. The case with the probe is on the right figure. Here, the pressure on the front face is also constant, and the amplitude is  $1.03 \mu N \cdot cm^{-2}$ . The standard deviation of this pressure is  $0.04 \mu N \cdot cm^{-2}$ . Therefore, the difference between both simulations remains within the computing error. In contrast, there is pressure on the back face of the sensor. This pressure varies linearly from  $0.75 \mu N \cdot cm^{-2}$  near the axis to  $0.95 \mu N \cdot cm^{-2}$  at the edge of the sensor.

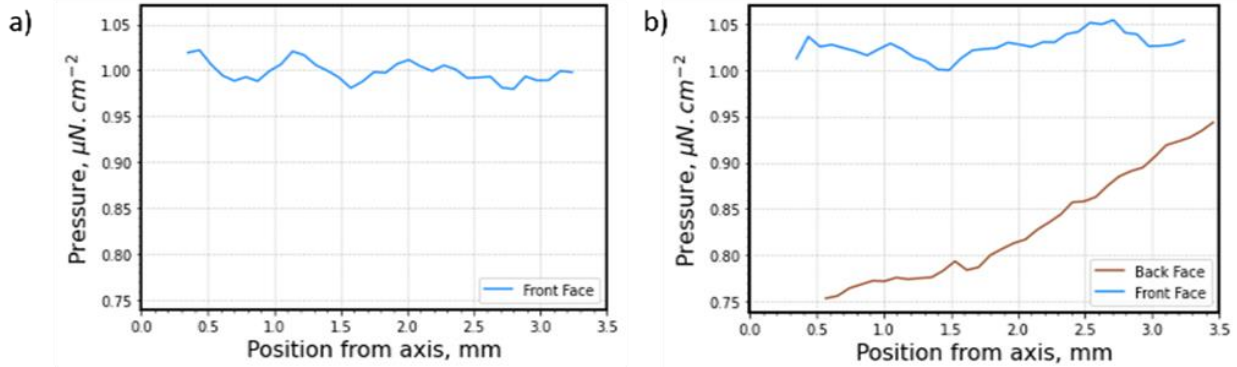


Figure 10: Left: Pressure on the front face of the sensor in the case where there is only the sensor in the gas plume.(Fig 9b) Right: Pressure on the back face and the front face of the sensor when there is a casing around the sensor (Fig 9c)

At the same position, Figure 11 shows the gas pressure without the presence of the sensor or the probe case. This pressure is computed at a virtual surface at the same position as the probe. In this figure, we can see the pressure between the axis and 10cm from the axis. Near the axis, the total pressure remains nearly constant such as  $P=0.59 \mu N \cdot cm^{-2}$ . This pressure is mainly due to the dynamic pressure term  $\rho u^2$ . When the radial distance increases, the pressure of the gas decrease to reach  $0.1 \mu N \cdot cm^{-2}$  at 9cm. After, the pressure collapses due to the vacuum tank edge effect. Table 1 summarizes the pressure at the different surfaces for each case studied. We can see that the pressure at the virtual surface without a probe is nearly half the pressure at surface 1 for the cases with the sensor and the case. There is no surface in this case; therefore, there is no pressure on the Surface 1 and 2. Surface 1 sees the same pressure with the sensor and with the probe.

Table 1: This table presents the pressure at the surfaces and at the virtual surface for each case studied

	Virtual surface	Surface 1	Surface 2
Without sensor	$0.59 \mu N \cdot cm^{-2}$	-	-
With sensor	-	$1.00 \mu N \cdot cm^{-2}$	$0 \mu N \cdot cm^{-2}$
With probe	-	$1.03 \mu N \cdot cm^{-2}$	$0.75-0.95 \mu N \cdot cm^{-2}$

The pressure on surface 2 comes from the casing located behind the sensor. Indeed, the particles bounce against the complex surface of the casing, and are reflected in the direction of the surface 2. The casing is constituted of an opening in its center to evacuate the particles. One can ask how can the dimensions of this opening change the pressure on the surface 2. Four cases with different opening dimensions have been simulated. The opening went from a radius of 1mm to a radius of 4mm. As the pressure in the Surface 2 is not constant, we integrated this pressure over the surfaces to get the force induced by the particles. As a result, Figure 12 shows force F1 on surface 1, F2 on surface 2, and the differential between both forces. One can see that the force on the surface 1 is constant even if the size of the case behind it changes. However, the significant change comes from the force on the surface 2. As the aperture on the case increase, fewer particles bounce back to the surface 2. Therefore, the pressure on the back face decreases, and the differential force increases.

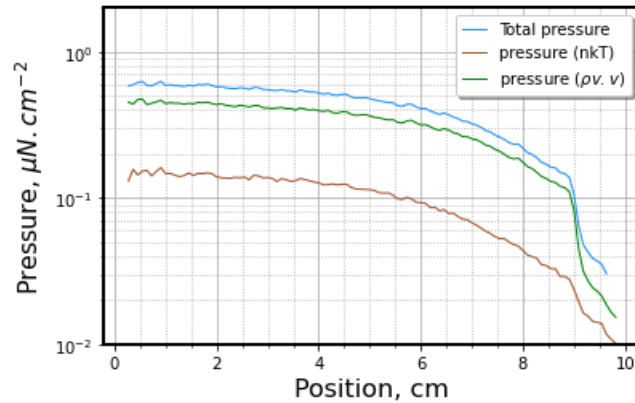


Figure 11: Gas pressure along the radial axis at 13cm from the source, Fig 9c).

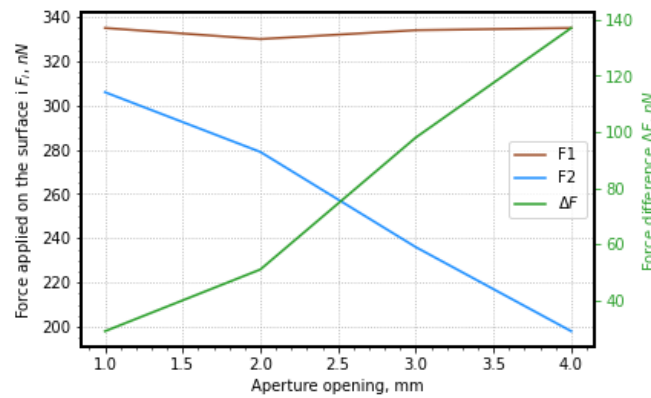


Figure 12: Force applied on the surface 1 and 2 for different opening in the case

## 2. Discussion

In the experiment, the estimated pressure from an order of magnitude analysis is  $66\mu N.cm^{-2}$  (eq 5). At 13cm downstream of the aperture, the pressure drops because the section of the pipe  $A$  is greater than the aperture one  $A^*$ . If the gas takes all the volume of the vacuum tank uniformly, then the pressure is estimated to

$$P_{13cm} = P^* \frac{A^*}{A} = 0.19\mu N.cm^2 \quad (13)$$

This pressure is in the same order of magnitude as the one measured. However, this rough estimation cannot be used to characterize the sensor's performance. Indeed, the gas pressure is not uniform over the pipe section. As we see in the measurement, the pressure is bell-shaped along a radial axis. Furthermore, the pressure has a square root link to the temperature. This gas temperature could be lower than the estimated room temperature because of gas expansion inside the buffer reservoir. To understand the experimental results, the experimental pressure measurement was normalized, and compared to the normalized simulation results (Fig 9a). In Figure 13, we can see that the shape of both simulation and experimental measurement are the same. The simulation is noisier near the axis because of the axisymmetric simulation. In this type of simulation, there are fewer particles near the axis. Nevertheless, both the measurement and the simulation show a maximum at the axis. The pressure decrease when the probe moves radially. Unfortunately, because of the vacuum tank size, it was not possible to measure the pressure at radial position greater than 5cm.

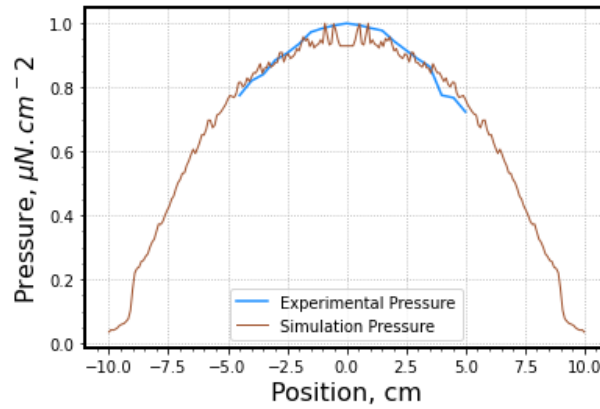


Figure 13: Normalized experimental and simulated pressure at 13cm from the source

Now, we take the pressure at the axis to compare the experimental and simulated absolute pressure. For the simulation, the pressure at the virtual surface (Fig 9a) is nearly half the pressure when there is a surface. This can be explained easily in Figure 7. In the virtual surface case, only incident particles create pressure. In the case of a surface, there is a pressure from the incident particles and a pressure from the reflected particles. In the following equation, we write the pressure according to their velocity distribution. The term  $f_1^+$  is the Boltzmann distribution of incident particles and  $f_1^-$  is the distribution of reflected particles. In the specular case, the reflected distribution is the same as the incident one. Therefore, the pressure is two-time the pressure without the sensor. In the diffusive case, the particles are accommodated on the surface. This means that the velocity of the reflected particles has a distribution centered around the surface temperature. Here, as the surface and source temperatures are the same, the pressure in the normal direction from the reflected particles is lower than the one from incoming particles. Therefore, the pressure is less than two times the virtual case pressure. Most of the time, particle-surface interaction is more diffusive than specular [16].

$$\vec{P}_1 \cdot \vec{n}_1 = - \int m v^2 f_1^+ d\vec{v} - \int m v^2 f_1^- d\vec{v} \quad (14)$$

We analyze the pressure on Surface 2. In the case of the sensor (Fig 9b), there is no pressure in this face. Indeed, particles come from the source and hit only the pipe and the Surface 1. There is no possible way to hit directly or indirectly Surface 2. On the contrary, the case with the probe (Fig 9c) presents a few surfaces downstream of the sensor. Particles from the source can bounce back on these surfaces of the probe and be directed to the Surface 2. They bounce again and remain stuck between the probe and the sensor. After a few back and forth motions, particles can escape through the probe's aperture or the aperture between the probe and the sensor. This behavior results in high pressure on the surface 2. It is also responsible for the difference in pressure between the axial position on surface 2 and the farthest point of the sensor from the axis. The former position sees fewer particles and so has lower pressure applied. On the contrary, the probe encapsulates the latter. Many particles hit this part of the surface 2. It results in pressure between  $0.75 \mu N \cdot cm^{-2}$ , and  $0.95 \mu N \cdot cm^{-2}$ . This pressure is relatively high compared to the pressure on the surface 1, this pressure is roughly 75% to 95% of the front pressure. The pressure varies according to position, so comparing the total force applied on each surface is easier. The resulting forces are  $F_1 = 330 nN$  and  $F_2 = 279 nN$ , respectively on surface 1 and on surface 2. The difference between both these forces is then  $\Delta F = 51 nN$ . In the experiment, we measure this difference directly. The equivalent force is  $\Delta F_{exp} = 105 nN$ . The measured force is two-times the simulated force. Nevertheless, the order of magnitude is respected, but the results remain different. The aperture radius is currently 2mm. However, when the radius is 3mm, the forces differences in the simulation increase to 98nN. It shows two things. First, the differential forces in the simulation are near the experimental force. Two, the probe dimension has a significant influence on the results. Indeed, the force difference between both surfaces is proportional to the aperture size. This size is no more precise in the experiment than half a millimeter.

One solution to limit the backflow effect is to have an aperture greater than the sensor. However, this is not technically possible. Another possible way is to remove the casing around the proof mass but keep it around the sensitive part of the sensor. For this purpose, it is necessary to redesign a new probe.

### 3. Conclusion

A new sensor has been developed to measure the thrust of the satellite's electric propulsion. This sensor is placed inside the plasma plume when the thruster is located inside a vacuum tank on the ground. Such a sensor undergoes harsh conditions to measure forces as low as a few nanoNewtons. In this paper, we studied the probe sensitivity in a less stringent case, using a neutral gas source. We mounted a gas source experiment and measured its downstream pressure. To understand the local behavior of the gas, we simulated this experiment in DS2V, a direct Monte Carlo simulation. We showed that the pressure measured is greater than the one without a diagnostic probe because of the transfer in particle momentum to the sensor.

Furthermore, we found the same results in the simulation as in the experiment, only when the casing around the sensor was modeled. Indeed, there is an important influence of the casing protecting the sensor. Particles from the source can bounce on the casing and create pressure on the back face of the sensor. The resulting force measured is much lower than the one expected. Additionally, it varies significantly in function of the shape of the casing. One solution to limit the casing's influence is to work on a new casing designed to limit particle bouncing back to the sensor. The next step in the simulation is to use a Particle in Cell (PIC) code to simulate charged particles. This will introduce the plasma effect we cannot see in a neutral gas, such as the sheath and electrostatic pressure.

### References

- [1] A. Spethmann, T. Trottenberg, and H. Kersten, "Spatially Resolved Momentum Flux Measurements for Thruster Plume Diagnostics," presented at the IEPC, 2013.
- [2] J. E. Polk *et al.*, "Recommended Practice for Thrust Measurement in Electric Propulsion Testing," *J. Propuls. Power*, vol. 33, no. 3, pp. 539–555, May 2017, doi: 10.2514/1.B35564.
- [3] B. W. Longmier *et al.*, "Validating a Plasma Momentum Flux Sensor to an Inverted Pendulum Thrust Stand," *J. Propuls. Power*, vol. 25, no. 3, pp. 746–752, May 2009, doi: 10.2514/1.35706.
- [4] H. Zhang, D. T. Li, F. He, and X. W. Chen, "Development of an indirect thrust stand based on a cantilever beam," *AIP Adv.*, vol. 11, no. 3, p. 035006, Mar. 2021, doi: 10.1063/5.0041530.
- [5] M. D. West, C. Charles, and R. W. Boswell, "A high sensitivity momentum flux measuring instrument for plasma thruster exhausts and diffusive plasmas," *Rev. Sci. Instrum.*, vol. 80, no. 5, p. 053509, May 2009, doi: 10.1063/1.3142477.
- [6] T. Trottenberg, A. Spethmann, J. Rutscher, and H. Kersten, "Non-electrostatic diagnostics for ion beams and sputter effects," *Plasma Phys. Control. Fusion*, vol. 54, no. 12, p. 124005, Dec. 2012, doi: 10.1088/0741-3335/54/12/124005.
- [7] S. Chakraborty, D. G. Courtney, and H. Shea, "A 10 nN resolution thrust-stand for micro-propulsion devices," *Rev. Sci. Instrum.*, vol. 86, no. 11, p. 115109, Nov. 2015, doi: 10.1063/1.4935471.
- [8] D. Seo, Y. Ryu, J. Choi, and J. Lee, "Design, fabrication, and calibration of a micro-load cell for micro-resistojet development," *Rev. Sci. Instrum.*, vol. 92, no. 11, p. 115002, Nov. 2021, doi: 10.1063/5.0059081.
- [9] P.-Q. Elias, R. Levy, J. Jarrige, V. Gaudineau, and C. Boniface, "Thrust measurements using plasma pressure measurements in the plume a feasibility," presented at the IEPC2019,
- [10] S. ASTRUC, P.-Q. Elias, R. Levy, and V. Gaudineau, "Thrust measurement using a plasma pressure probe immersed in the plume," presented at the International Electric Propulsion Conference 2022,
- [11] R. Levy, D. Janiaud, J. Guerard, R. Taibi, and O. L. Traon, "A 50 nano-g resolution quartz Vibrating Beam Accelerometer," in *2014 International Symposium on Inertial Sensors and Systems (ISISS)*, Laguna Beach, CA, USA: IEEE, Feb. 2014, pp. 1–4. doi: 10.1109/ISISS.2014.6782532.
- [12] S. Candel, *Mécanique des fluides: cours*, 2e éd. [nouv. présentation]. in Sciences sup. Paris: Dunod, 2001.
- [13] J. M. Lafferty, Ed., *Foundations of vacuum science and technology*. New York: Wiley, 1998.
- [14] G. A. Bird, *The DSMC method*, Version 1.2. S.I.: G. A. Bird, 2013.
- [15] G. C. Soulas, "Gas Flux and Density Surrounding a Cylindrical Aperture in the Free Molecular Flow Regime," 2011.
- [16] L. Liu, G. Cai, H. Zheng, S. Shang, and B. He, "Measurement of the momentum accommodation coefficient for the interactions between electric thruster plume and a solid surface," *Phys. Plasmas*, vol. 27, no. 5, p. 053511, May 2020, doi: 10.1063/5.0004874.